Electronic Supplementary Material (ESI) for Environmental Science: Nano.

Supporting Information for:

Complementary Colloid and Collector Nanoscale Heterogeneity Explains Microparticle Retention Under Unfavorable Conditions

Cesar A. Ron[1], William P. Johnson[1,*]

[1]Department of Geology & Geophysics, University of Utah, Salt Lake City, UT 84112, USA

*Email: william.johnson@utah.edu. Tel.: +1 801 585 5033.

Content

Distribution of heterodomains on the collector used in Ron et al. (2019).

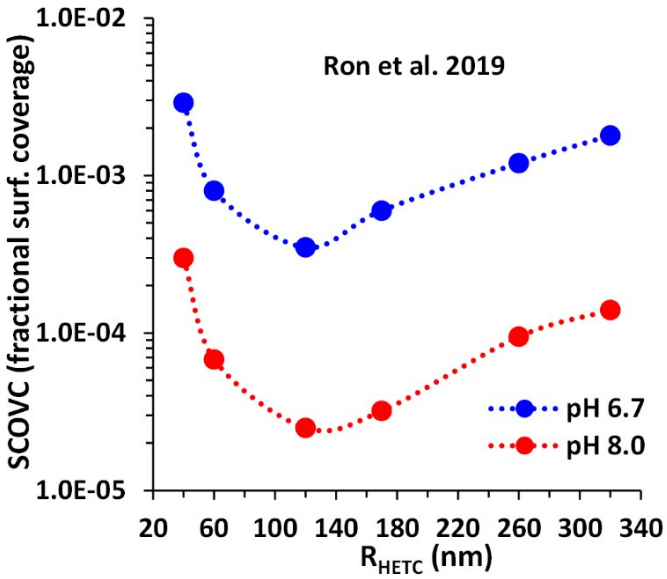

Figure SI-1. Closed circles correspond to distribution of surface coverage (SCOVC) versus radius (R_{HETC}) of heterodomains on the collector (HETC) as used in Ron et al.[1]

Impinging jet system

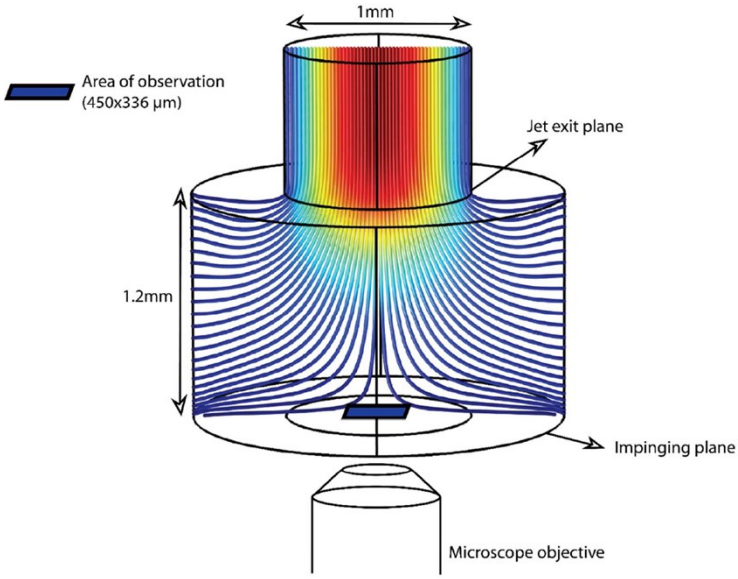

Figure SI-2. Schematic of the impinging jet flow chamber. Fluid flow field is represented by color coded low lines (red high velocity, blue low velocity). The jet is 0.5 mm in radius and the impinging plane is located 1.25 mm below the jet exit. Images of attached colloids are acquired *via* an inverted microscope across an area of observation of 450x336 µm on the impinging plane aligned with the center of the jet.[2–4]

Methods

Projecting heterodomains on the colloid to the collector surface

Heterodomains on the colloid (HETP) were distributed as spherical caps of surface area A_{HETP} and arc length equal to $2R_{HETP}$ (Figure SI-3).

$$A_{HETP} = 2\pi a_P^2(1 - cos\omega_0)$$

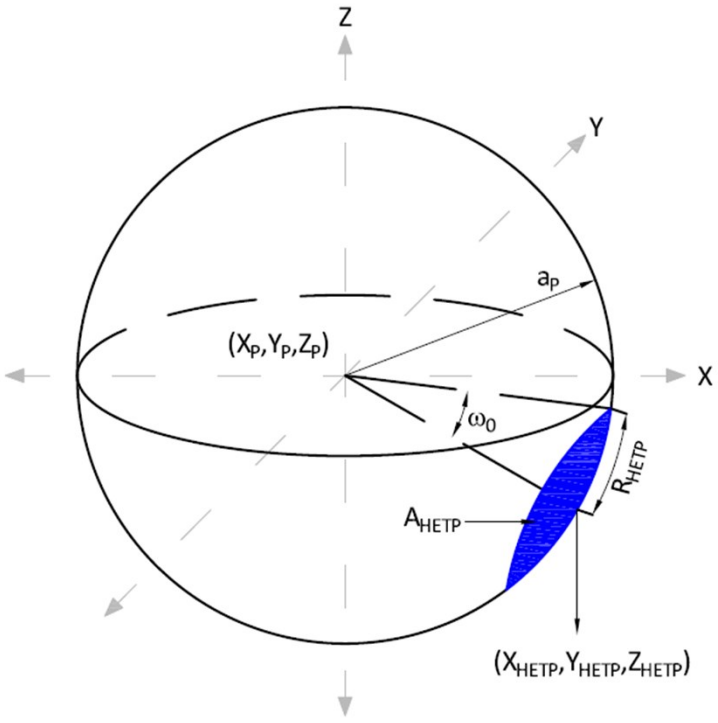

Figure SI-3. 3D representation of a colloid hosting a HETP.

The center of the HETP projection (X_{HETPr},Y_{HETPr}) onto the collector is determined as follows (Figures SI-4 and SI-5):

$$\beta = \cos^{-1}\left(\frac{Z_P - Z_{HETP}}{a_P}\right)$$

$$D_{AP} = a_P - a_P'$$

$$D_C = D_{AP}sin\beta$$

$$D_X = D_C cos\varphi$$

$$D_Y = D_C sin\varphi$$

$$X_{HETPr} = X_{HETP} + D_Y$$

$$Y_{HETPr} = Y_{HETP} + D_Y$$

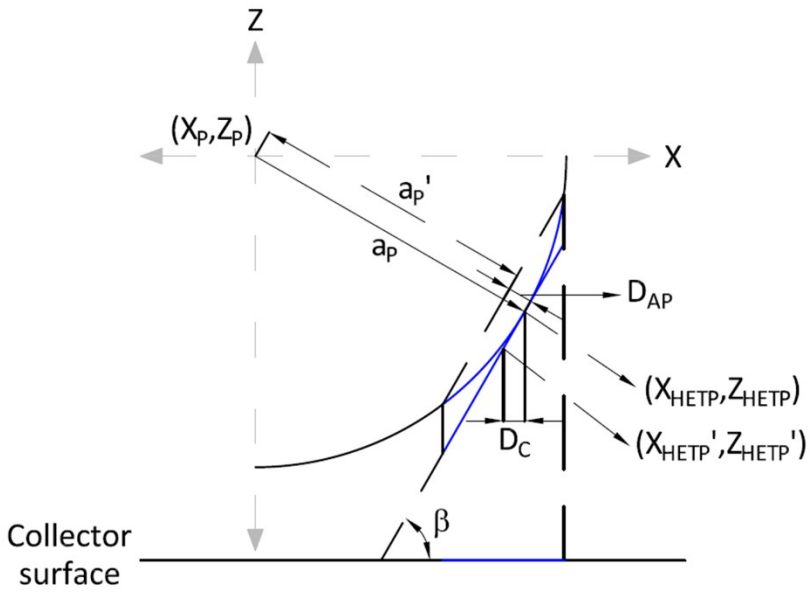

Figure SI-4. Center displacement as consequence of projecting HETP. View over X-Z plane.

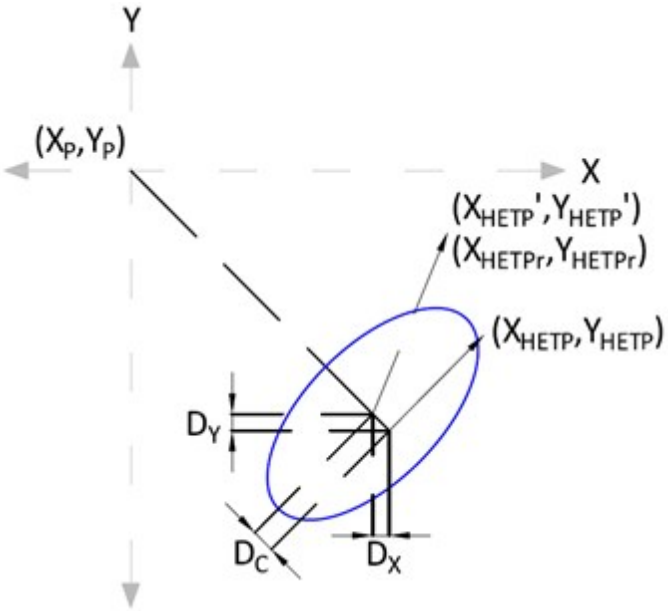

Figure SI-5. Center displacement as consequence of projecting HETP. View over X-Y plane.

The projection of a HETP onto the collector surface corresponds to an ellipse with major and minor diagonals a_{HETPr} and b_{HETPr}, respectively (major and minor diagonals are of equal value if the heterodomain center lies on the z-axis). The major (a_{HETPr}) and minor (b_{HETPr}) diagonals are determined as follows (Figures SI-6 to SI-9):

$$\omega_0 = \frac{R_{HETP}}{a_P}$$

$$R_{HETP}' = a_P sin\omega_0$$

$$a_{HETPr} = R_{HETP}'$$

$$b_{HETPr} = R_{HETP}' cos\beta$$

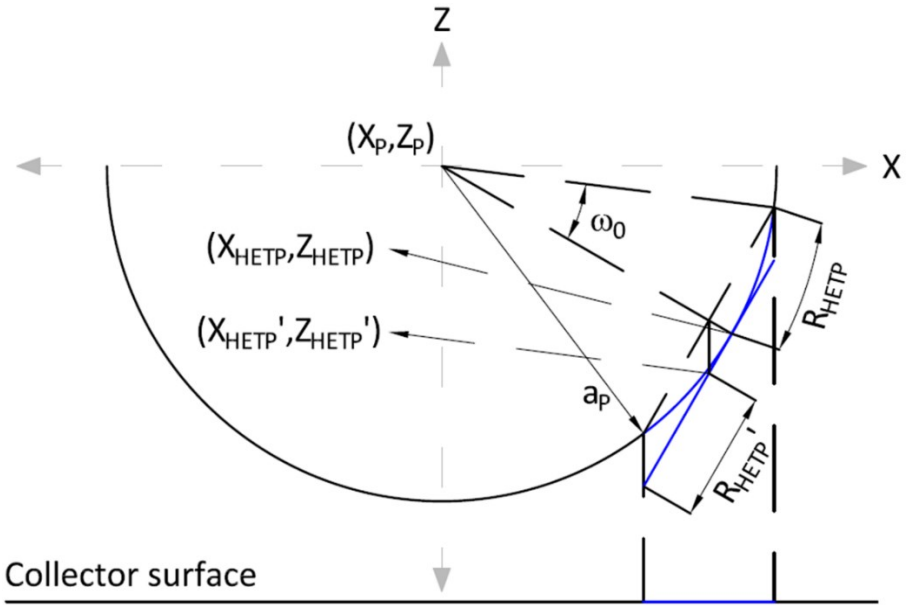

Figure SI-6. R_{HETP} reduces to $R_{HETP'}$ when projecting HETP. View over X-Z plane.

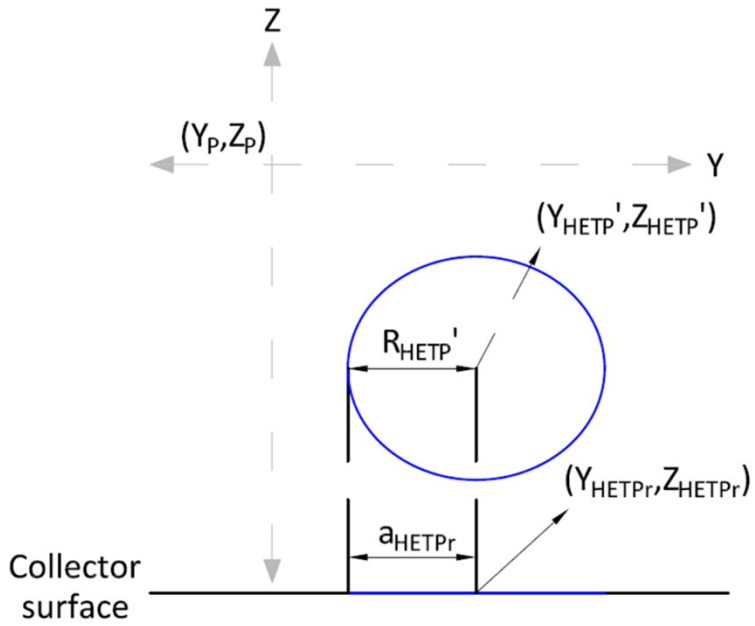

Figure SI-7. Determination of major diagonal of projected HETP. View over Y-Z plane.

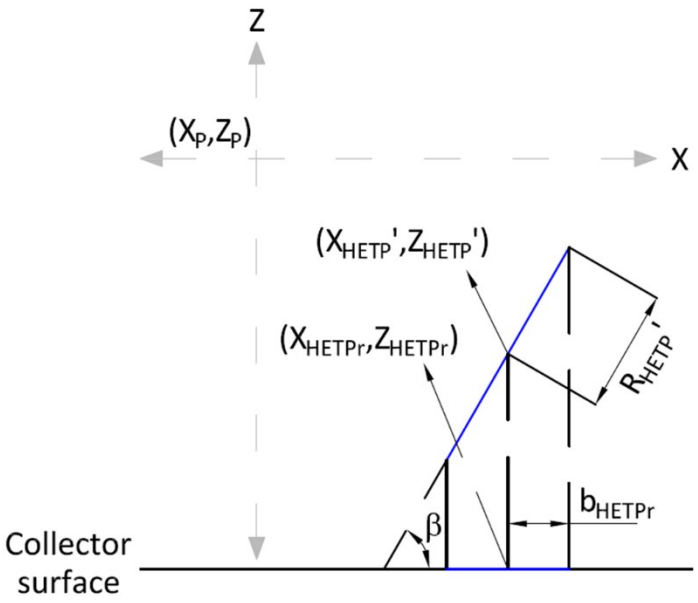

Figure SI-8. Determination of minor diagonal of projected HETP. View over X-Z plane.

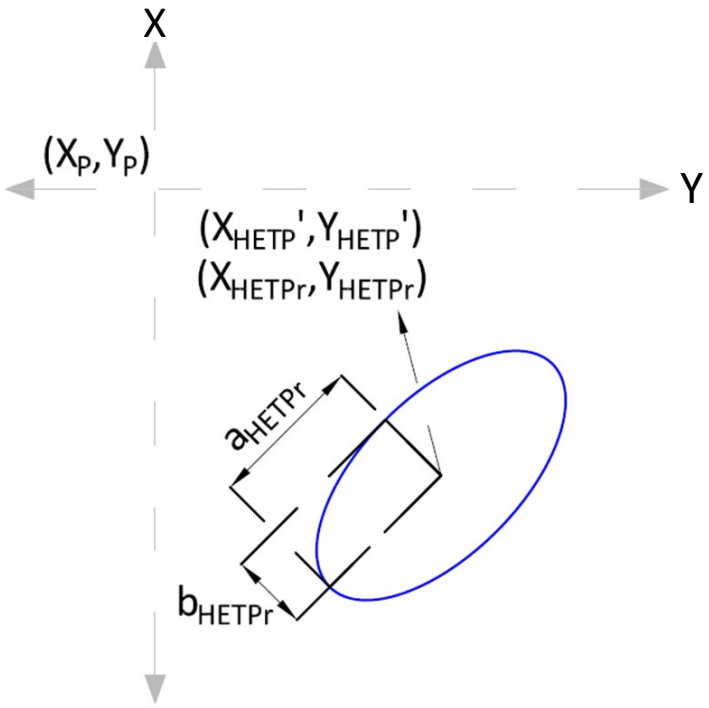

Figure SI-9. Determination of major and minor diagonals of projected HETP. View over X-Y plane.

To reduce mathematical complexity, HETP projections were approximated as circles of equivalent area and of radius R_{HETPr}.

$$R_{HETPr} = \sqrt{a_{HETPr} b_{HETPr}}$$

The validity of this approximation was demonstrated *via* the discrepancy on radius of curvature for a circular HETP projection (Rc) relative to an elliptical HETP projection (Re, radius of curvature at vertices of the minor diagonal) (Figure SI-10a). This discrepancy was determined as a function of radial distance of heterodomain projection center from colloid center ($D_{HETPr-P}$) normalized to colloid radius (a_p) (Figure SI-10b, blue). In this study, we only considered the projection of those HETP partially or fully encompassed by the zone of interaction (ZOI) (Figure SI-2), therefore the maximum discrepancies corresponded to HETP projected at radial distances equal to one ZOI radius plus one HETP projection radius. As example, if a 5 nm heterodomain placed on a 0.11 μm colloid is projected at a distance equal to the ZOI radius (R_{ZOI}, 29.41 nm, IS 6.0 mM) (Figure SI-10a), the discrepancy on radius of curvature is 1.3% (Figure SI-10b, red).

$$Discrepancy = \frac{R_e - R_c}{R_e}(100\%)$$

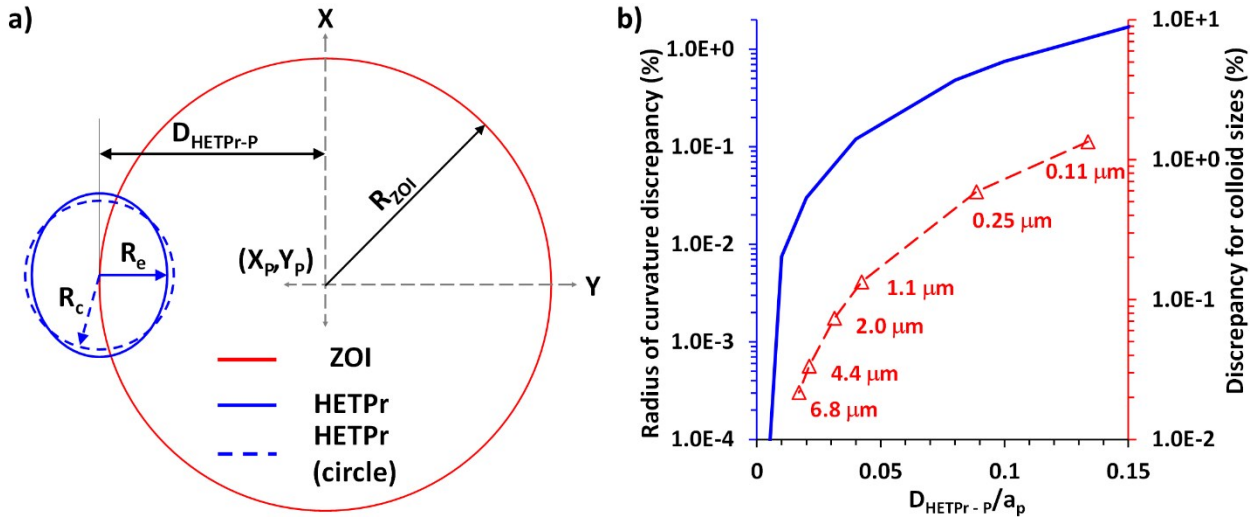

Figure SI-10. a) Representation of HETP projected at a distance equal to one R_{ZOI}. The discrepancy on radius of curvature for a circular HETP projection (Rc) relative to an elliptical HETP projection (Re, radius of curvature at vertices of the minor diagonal) is depicted. **b)** Radius of curvature discrepancy as a function of radial distance between heteorodomain projection center and colloid center ($D_{HETPr-P}$) normalized to colloid radius (a_p) (blue). Radius of curvature discrepancy for HETP projected at one ZOI radius from colloid center under 6 mM IS conditions (red).

Angles defining colloid orientation

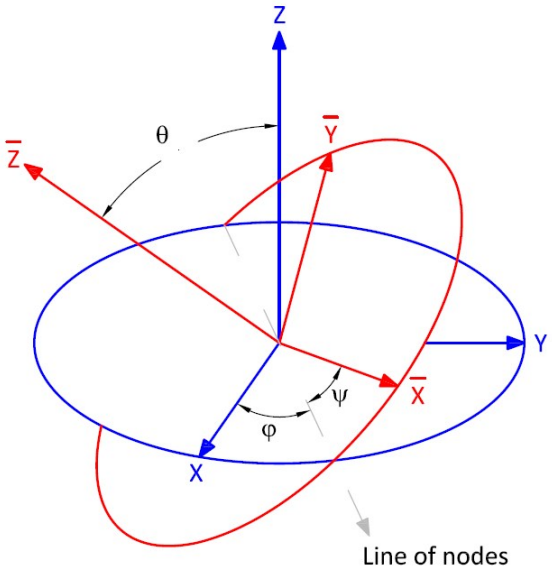

Figure SI-11. Representation of the three Euler angles that define colloid orientation in a 3D space.

Limits on surface coverage (SCOVP) and radius (R_{HETP}) of heterodomains on colloid (HETP)

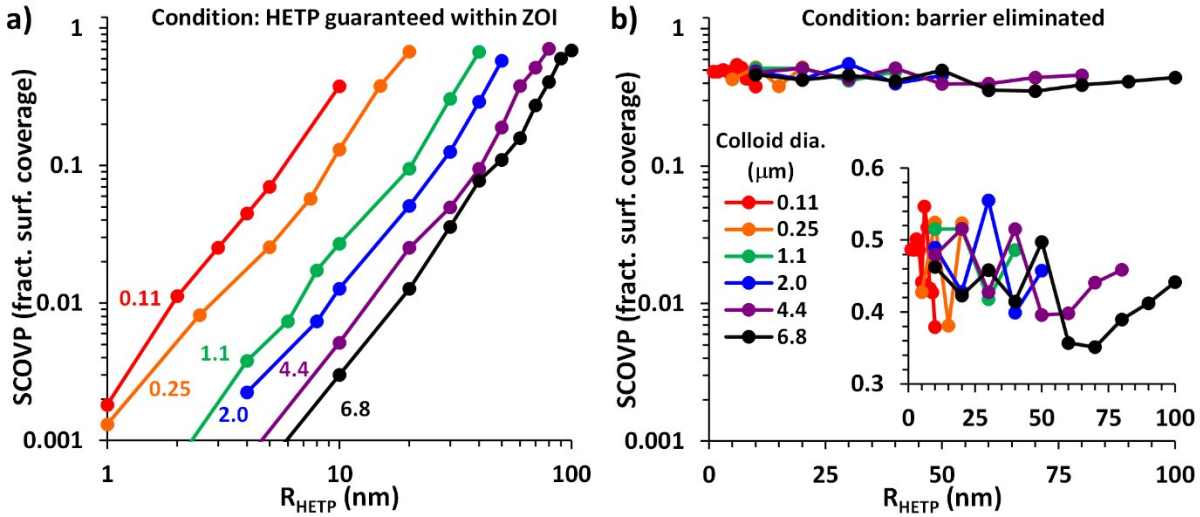

Figure SI-12. a) Surface coverage (SCOVP) as a function of radius (R_{HETP}) of heterodomain on colloid (HETP) that guarantees that at least one HETP will be completely encompassed by the ZOI regardless of colloid orientation (rotation). **b)** SCOVP as a function of R_{HETP} that eliminates XDLVO energy barrier solely by HETP (HETC absent). The variability of SCOVP reflects discrete steps used for RHETP (1 nm to 10 nm) and discrete percent change (10%) for SCOVP. For both panels conditions were IS 6.0 mM and pH 8.0.

Representation of DRNH on collector and colloid as utilized in mechanistic trajectory simulations

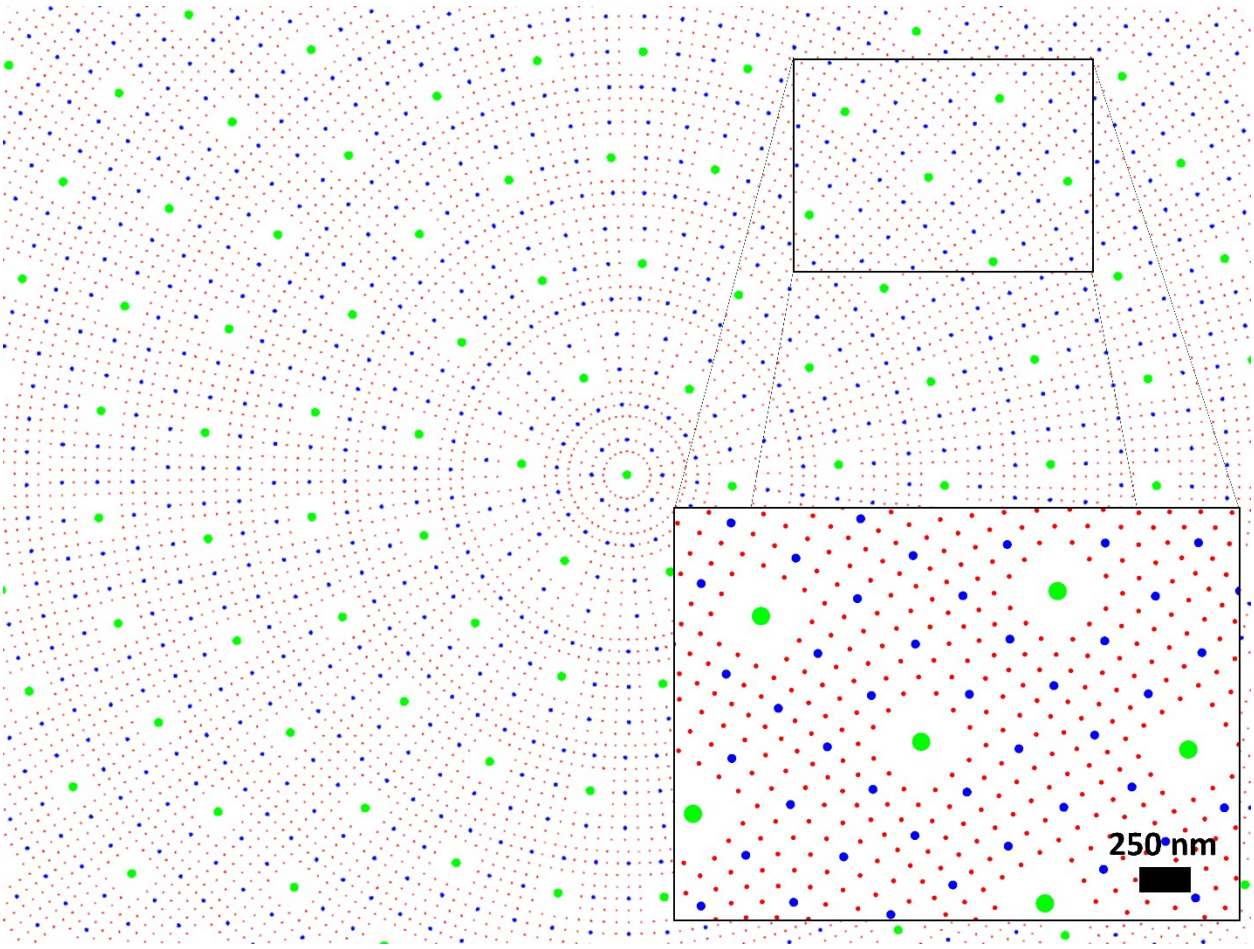

Figure SI-13. Representation of DRNH on the collector surface. HETC were represented by three R_{HETC}: 90 (green), 45 (blue) and 25 (red) nm with spatial frequency ratios of 1, 8, and 64, respectively. All three HETC were present on the simulated collector surface. In this representation SCOVC was increased for visualization purposes.

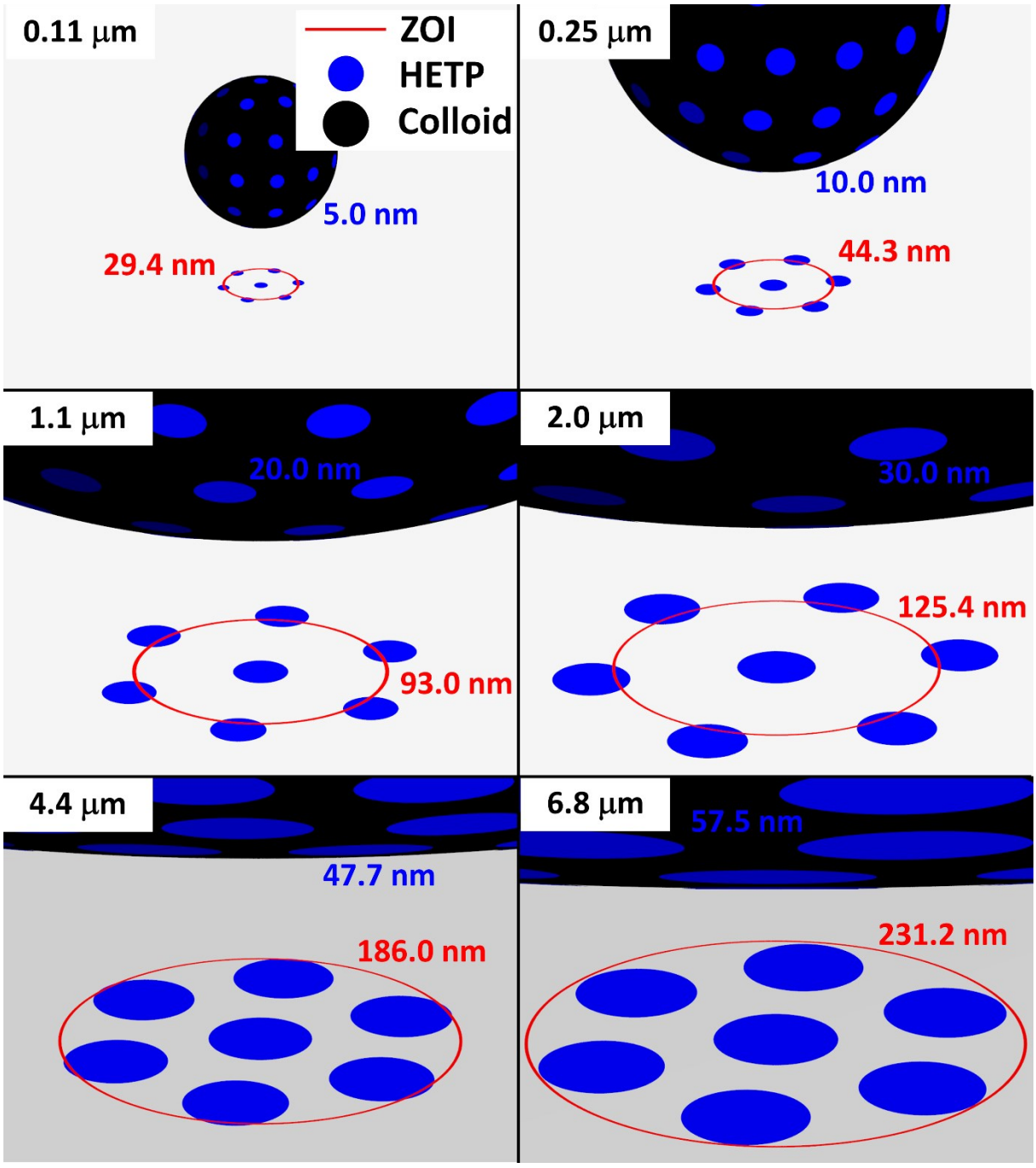

Figure SI-14. Representation of DRNH on the colloid surface. For each colloid size, HETP (blue) were of a given size (R_{HETP}) and were placed at values of SCOVP as described in the power-law distribution (Figure 4a and d) utilized in mechanistic trajectory simulations. The ZOI is represented by the red circle and conditions were IS 6.0 mM and pH 8.0.

Machine learning clustering analysis

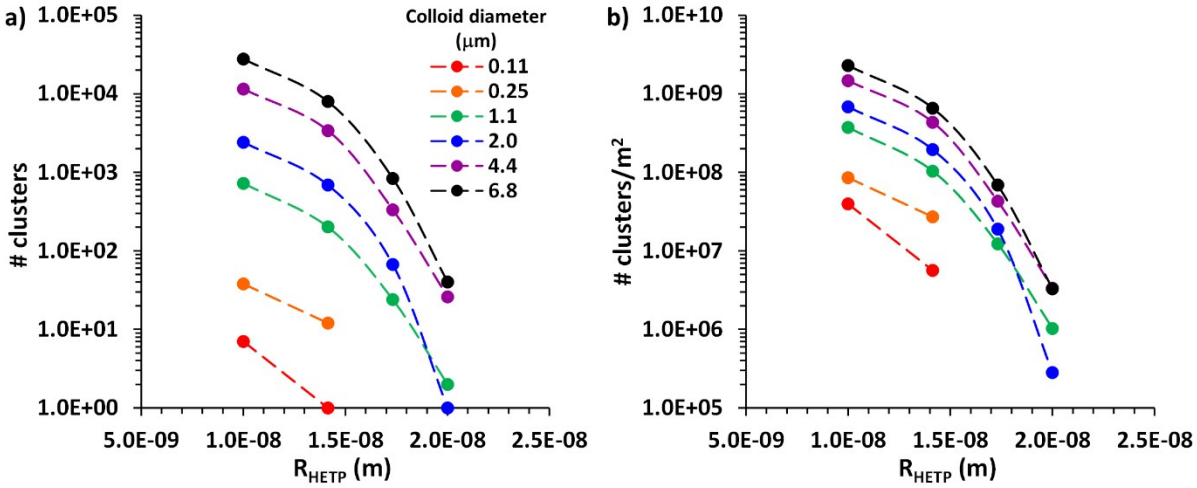

Figure SI-15. Distributions of cluster R_{HETP} obtained by randomly placing (specifying no overlap) primary heterodomains of 10 nm radius, on an area equivalent the colloid surface area, and at a fractional SCOVP of 0.1. Based on the initial position of the primary heterodomains, the machine learning clustering algorithm (agglomerative clustering, from Scikit Learn library in Python) determines the R_{HETP} and number of clusters formed when primary heterodomains are within a threshold separation distance (10 nm). While the primary-sized heterodomains are depleted by clustering, larger sizes follow a power law distribution. Similar results were obtained by repeating the analysis for other values of RHETP (10 and 20 nm), SCOVP (0.2 and 0.4), and threshold separation distance (5, 10 and 20 nm).

ζ-potential and roughness for CML and soda-lime glass (silica)

Table SI-1. ζ-potential values used in simulations for carboxylate modified polystyrene latex nano- and microspheres (CML). Values were determined from EPM measurements *via* the Smoluchowski equation.[5] Note that measurements for colloids > 2.0 μm have inherent uncertainty using this method.

Material	Colloid Diameter (μm)	NaCl (mM)	pH	ζ-potential (mV)
CML	0.11	6.0	6.7	-45.3
CML	0.25	6.0	6.7	-18.3
CML	1.1	6.0	6.7	-65.4
CML	2.0	6.0	6.7	-29.9
CML	4.4	6.0	6.7	-65.0
CML	6.8	6.0	6.7	-10.2
CML	0.11	20.0	6.7	-35.9
CML	0.25	20.0	6.7	-10.5
CML	1.1	20.0	6.7	-50.1
CML	2.0	20.0	6.7	-8.2
CML	4.4	20.0	6.7	-42.8
CML	6.8	20.0	6.7	-4.5
CML	0.11	6.0	8.0	-61.4
CML	0.25	6.0	8.0	-74.9
CML	1.1	6.0	8.0	-91.0
CML	2.0	6.0	8.0	-80.5
CML	4.4	6.0	8.0	-52.0
CML	6.8	6.0	8.0	-6.9
CML	0.11	20.0	8.0	-42.0
CML	0.25	20.0	8.0	-26.5
CML	1.1	20.0	8.0	-62.2
CML	2.0	20.0	8.0	-63.9
CML	4.4	20.0	8.0	-63.1
CML	6.8	20.0	8.0	-11.8
CML	0.11	50.0	2.0	-13.8
CML	0.25	50.0	2.0	-2.3
CML	1.1	50.0	2.0	-5.1
CML	2.0	50.0	2.0	-5.4
CML	4.4	50.0	2.0	-11.7
CML	6.8	50.0	2.0	1.9

Table SI-2. ζ-potential values used in simulations for soda-lime glass collector surface (silica). ζ-potential were from representative values reported in the literature.

Material	NaCl (mM)	pH	ζ-potential (mV)
Glass[6]	6.0	6.7	-70.0
Glass[6]	20.0	6.7	-53.5
Glass[6]	6.0	8.0	-80.0
Glass[6]	20.0	8.0	-70.0
Glass[7]	50.0	2.0	-10.0

Table SI-3. RMS roughness values used in simulations regarding attachment of CML onto silica surfaces. Roughness values were determined as described in Rasmuson et al.[8]

CML diameter (μm)	RMS roughness (nm)
0.11	4.7
0.25	6.4
1.1	10.3
2.0	13.0
4.4	17.0
6.8	19.8

References

1 C. A. Ron, K. VanNess, A. Rasmuson and W. P. Johnson, How nanoscale surface heterogeneity impacts transport of nano- to micro-particles on surfaces under unfavorable attachment conditions, *Environ. Sci. Nano*, 2019, **6**, 1921–1931.

2 E. Pazmino, J. Trauscht, B. Dame and W. P. Johnson, Power Law Size-Distributed Heterogeneity Explains Colloid Retention on Soda Lime Glass in the Presence of Energy Barriers, *Langmuir*, 2014, **30**, 5412–5421.

3 J. Trauscht, E. Pazmino and W. P. Johnson, Prediction of Nanoparticle and Colloid Attachment on Unfavorable Mineral Surfaces Using Representative Discrete Heterogeneity, *Langmuir*, 2015, **31**, 9366–9378.

4 A. Rasmuson, E. Pazmino, S. Assemi and W. P. Johnson, Contribution of Nano- to Microscale Roughness to Heterogeneity: Closing the Gap between Unfavorable and Favorable Colloid Attachment Conditions, *Environ. Sci. Technol.*, 2017, **51**, 2151–2160.

5 H. Ohshima, Electrophoresis of soft particles: Analytic approximations, *Electrophoresis*, 2006, **27**, 526–533.

6 B. J. Kirby and E. F. Hasselbrink, Zeta potential of microfluidic substrates: 1. Theory, experimental techniques, and effects on separations, *Electrophoresis*, 2004, **25**, 187–202.

7 M. Tong and W. P. Johnson, Excess colloid retention in porous media as a function of colloid size, fluid velocity, and grain angularity, *Environ. Sci. Technol.*, 2006, **40**, 7725–7731.

8 A. Rasmuson, K. VanNess, C. A. Ron and W. P. Johnson, Hydrodynamic versus Surface Interaction Impacts of Roughness in Closing the Gap between Favorable and Unfavorable Colloid Transport Conditions, *Environ. Sci. Technol.*, 2019, **53**, 2450–2459.